Supplementary Material: A model of spatiotemporal regulation within biomaterials using DNA reaction-diffusion waveguides

S1. DNA Sequences and Purification

All DNA sequences used in well-mixed experiments were purchased from Integrated DNA Technologies (Coralville, IA).

Table S1. Waveguide Circuit DNA sequences.

Name	Sequence	Purification
Signal	CATTCAATAC CCTACG TCTCCA ACTAACTTACGG	Desalted
Output	ATCCACATACATCATATT CCCT CATTCAATAC CCTACG	Desalted
Carrier Bottom	GGAGA CGTAGG GTATTGAATG AGGG CCGTAAGTTAGT TGGAGA CGTAGG	Desalted
Sink Cover	CATTCAATAC CCTACG	Desalted
Sink Bottom	T TGGAGA CGTAGG GTATTGAATG	Desalted
Fuel	CCTACG TCTCCA ACTAACTTACGG CCCT CATTCAATAC CCTACG	Desalted
Reporter Bottom	TTGAATG AGGGAATATGATGTATGTGG/3IABKfQ/	HPLC
Reporter Cover	/56FAM/CCACATACATCATATT CCCT	HPLC
Clamped Output	CACATAACAA CCACATACATCATATT CCCT CATTCAATAC CCTACG CATACAA	Desalted
Clamped Signal	CACCATC CATTCAATAC CCTACG TCTCCA ACTAACTTACGG	Desalted
Clamped Carrier Bottom	TTGTATG GGAGA CGTAGG GTATTGAATG AGGG CCGTAAGTTAGT TGGAGA CGTAGG GATGGTG	Desalted

DNA complexes were annealed in 1X Tris-acetate-EDTA buffer with 12.5 mM Mg^{2+} (TAE/Mg^{2+} buffer). The annealing protocol consisted of heating the solution up to 90 °C for 5 minutes and then cooling 1 °C every minute to 20 °C in an Eppendorf Mastercycler. Annealed complexes were then PAGE (polyacrylamide gel electrophoresis) gel purified to remove single stranded impurities; the conditions were 15% PAGE gels run at 150 V for 3 hours. For the

Carrier complex, two bands were typically observed when visualized at 260 nm; a dark top band was positioned ¼ of the way down the total length of the gel, and a fainter thinner band was located ½ way down the gel length. The top band was cut from the gel and eluted in TAE/Mg^{2+} buffer for 1 day. The eluate was then centrifuged to remove small gel fragments from solution. For the Reporter and Sink complexes, one band was observed during PAGE gel visualization. These bands were cut from the gels, soaked in TAE/Mg^{2+} buffer for 1 day to elute the DNA, and centrifuged to remove small polyacrylamide fragments from solution.

S2. Well-Mixed Experiments

All well-mixed kinetic experiments were conducted using a Strategene MX3000 quantitative PCR machine at 25º C. We added reactants to 100 μL total volumes in individual wells of a 96-well plate. The concentrations of reactants listed in the main text are the final concentrations of the species in the 100 μL total volume. Each reaction well contained 1X TAE/Mg^{2+} buffer and 1 μM of PolyT20, a 20 nucleotide poly-thymine strand that acted as sacrificial DNA for adsorption to the polypropylene walls of the reaction wells. To initiate amplification reactions, reactants were added in the following order: Reporter, Carrier, Sink. A baseline fluorescence measurement was then made for 5 minutes. Finally, Fuel and Signal were added to trigger the reaction. In each experiment, each reaction condition was tested once.

S3. Modeling of Reaction-Diffusion Waveguides

Spatial models of reaction-diffusion waveguides were implemented using finite element analysis software using Comsol Multiphysics – Transport of Dilute Species node. The waveguide geometry was meshed with a combination of free tetrahedral and mapped element types. For the idealized waveguide, the model was composed of the following partial-differential equations:

$$\frac{\partial[Signal](t,x)}{\partial t} = D_{ss}\nabla^2[Signal]](t,x) + k_a[Signal](t,x)[Carrier](t,x) - k_d[Signal](t,x)[Sink](t,x)$$

$$\frac{\partial[Carrier](t,x)}{\partial t} = -k_a[Signal](t,x)[Carrier](t,x)$$

$$\frac{\partial[Sink](t,x)}{\partial t} = -k_d[Signal](t,x)[Sink](t,x)$$

Only Signal was allowed to diffuse and it was assigned a diffusion coefficient of 60 $\mu m^2\ s^{-1}$, which was the average value measured for a 43 nucleotide sized single stranded oligonucleotide in a 30% (v/v) poly(ethylene-glycol) diacrylate hydrogel[1]. The diffusion coefficients for all other species were set to 0. The full reaction-diffusion waveguide system consists of the following PDEs:

$$\frac{\partial[Signal](t,x)}{\partial t} = D_{ss}\nabla^2[Signal]](t,x) + 2k_i[Fuel](t,x)[Intermediate](t,x) + k_r[Output](t,x)[Intermediate](t,x)$$
$$- k_a[Signal](t,x)[Carrier](t,x) - k_T[Signal](t,x)[Sink](t,x)$$

$$\frac{\partial[Carrier](t,x)}{\partial t} = -k_a[Signal](t,x)[Carrier](t,x) + k_r[Output](t,x)[Intermediate](t,x) - k_{leak}[Fuel](t,x)[Carrier](t,x)$$

$$\frac{\partial[Sink](t,x)}{\partial t} = -k_T[Signal](t,x)[Sink](t,x)$$

$$\frac{\partial[Output](t,x)}{\partial t} = k_a[Signal](t,x)[Carrier](t,x) - k_r[Output](t,x)[Intermediate](t,x) - k_{rep}[Reporter](t,x)[Output](t,x)$$

$$\frac{\partial[Reporter](t,x)}{\partial t} = -k_{rep}[Reporter](t,x)[Output](t,x)$$

$$\frac{\partial[Intermediate](t,x)}{\partial t} = k_a[Signal](t,x)[Carrier](t,x) - k_i[Fuel](t,x)[Intermediate](t,x) - k_r[Output](t,x)[Intermediate](t,x)$$

$$\frac{\partial[Fuel](t,x)}{\partial t} = -k_{leak}[Fuel](t,x)[Carrier](t,x) - k_i[Fuel](t,x)[Intermediate](t,x)$$

$$\frac{\partial[Fluorophore](t,x)}{\partial t} = k_{rep}[Reporter](t,x)[Output](t,x)$$

The focus of our waveguide analyses was on the autocatalytic species, Signal. To mitigate computational cost and reduce convergence time, the reaction-diffusion network implemented in our Comsol model assumed that Output reacted with an infinitely large source of Reporter throughout the waveguide to instantaneously convert it to Fluorophore. Therefore, the model did not include the reporting reaction of Output and Reporter nor did it incorporate the reverse

reaction of Output and Intermediate. Reaction terms not modeled in the Comsol reaction-diffusion simulation are highlighted in purple in the system of PDEs listed above.

S4. Curve-fitting analysis of data from experiments on the amplifier in well-mixed solution

Kinetic models of the amplifier were implemented in MATLAB. All fluorescence data were converted from raw fluorescence intensity into Fluorophore concentration by calibrating each experiment. Calibration as performed by adding a known amount of Output to a concentration Reporter within separate individual reaction wells during the experiment. **Figure S2** shows a typical calibration plot. The calibration data allowed us to determine the average proportionality constant, χ, between the average change in fluorescence intensity and the amount of output added:

$$\langle \chi \rangle = \langle \frac{[Output]}{\Delta Counts} \rangle$$

$$[R_f(t)] = \langle \chi \rangle \Delta Counts(t)$$

We then used $\langle \chi \rangle$ to convert all fluorescence counts into Fluorophore concentration. Using this concentration time data, we performed nonlinear least-squares regression using the *lsqcurvefit* Matlab function, which varied reaction rate constants over a range of parameter values to minimize the sum of the square of the y-error between each measured experimental Fluorophore concentration and the Fluorophore concentration predicted by the model. Integration was performed using either the Runge-Kutta method or the variable step variable order method which were implemented using Matlab's *ode45* and *ode15s* functions[2].

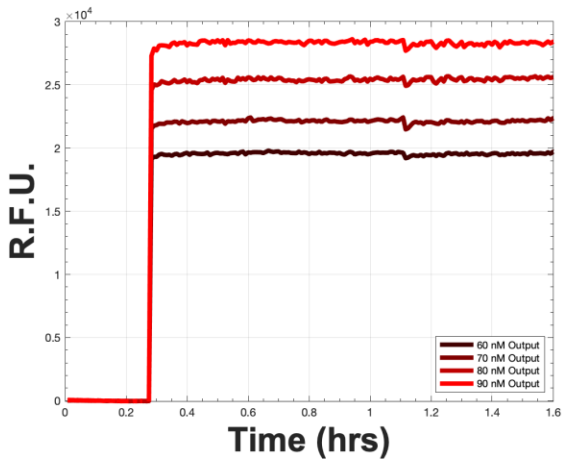

Figure S1. An example calibration plot in which different concentrations of Output added to each of 4 reaction wells containing 150 nM Reporter.

These models used the following ODEs describing the reaction rates of the system:

$$\frac{d[Signal](t)}{dt} = 2k_i[Fuel](t)[Intermediate](t) + k_r[Output](t)[Intermediate](t) - [Signal](t)[Carrier](t) - k_T[Signal](t)[Sink](t)$$

$$\frac{d[Carrier](t)}{dt} = -k_a[Signal](t,x)[Carrier](t,x) + k_r[Output](t,x)[Intermediate](t,x) - k_{leak}[Fuel](t,x)[Carrier](t,x)$$

$$\frac{d[Output](t)}{dt} = k_a[Signal](t)[Carrier](t) - k_r[Output](t)[Intermediate](t)$$

$$\frac{d[Reporter](t)}{dt} = -k_{rep}[Reporter](t)[Output](t)$$

$$\frac{d[Sink](t)}{dt} = -k_T[Signal](t)[Sink](t)$$

$$\frac{d[Intermediate](t)}{dt} = k_a[Signal](t)[Carrier](t) - k_r[Output](t)[Intermediate](t) - k_i[Fuel](t)[Intermediate](t)$$

$$\frac{d[Fuel](t)}{dt} = -k_{leak}[Fuel](t)[Carrier](t) - k_i[Fuel](t)[Intermediate](t)$$

$$\frac{d[Fluorophore](t)}{dt} = k_{rep}[Reporter](t)[Output](t)$$

The upper and lower bounds for the fitted rate constants were varied between 4E6 M^{-1} s^{-1} and 0 M^{-1} s^{-1}, covering the range of rate constants for bimolecular strand displacement reactions in standard buffer conditions at 25 ºC up to a maximum toehold size of 7 nucleotides.

When performing least-squares regression on the amplification perturbation experiments (main text section 3.3, **Figure 10**), our model first integrated the system of ODEs from the starting time to the time of perturbation. At this time point the model took the solution obtained

from integration and updated the concentration of Signal or Sink by adding 20 nM of the relevant species to its existing concentration. Numerical integration was continued from the perturbation time to the end of the experiment. The curve fitting function called this model for each specific time point and chose the set of rate constants that minimized the square of the y-error between the model and data set.

S5 Derivation of Fisher-Kolomogorov-Petrovsky-Piskunov Equation for an autocatalytic wavefront

For a one-dimensional system, the reaction-diffusion equation describing the accumulation of Signal (abbreviated as Sg below) within the wire over space and time is:

$$\frac{\partial Sg(x,t)}{\partial t} = D_{Sg}\frac{\partial^2 Sg(x,t)}{\partial x^2} + r\big(Sg(x,t)\big) \quad (1)$$

where D_{Sg} is the diffusion coefficient of Signal and r(Sg) is the net reaction rate of Signal, and x is the semi-infinite spatial domain which extends from x_1. The initial conditions of the system are:

$$Sg(x,0) = 0 \text{ for all } x < x_1$$

$$Sg(x,0) = Sg_{max} \text{ for all } x \geq x_1$$

The growth rate of Signal is assumed to be bounded:

$$r(Sg_{max}) = 0 \text{ and } r(0) = 0$$

Finally, several restrictions are placed on the growth rate of Signal. First, the reaction rate is assumed to be positive when $0 < Sg(x,t) < Sg_{max}$:

$$r(Sg) > 0$$

Second, the derivative of the reaction rate must satisfy the following inequalities:

$$r'(0) > 0$$

$$r'(Sg) < r'(0) \text{ when } 0 < Sg(x,t) \leq Sg_{max}$$

Far field conditions for the solution to the PDE are:

$$Sg(x,t) \xrightarrow[x \to -\infty]{} 0 \text{ and } Sg(x,t) \xrightarrow[x \to +\infty]{} Sg_{max}$$

We then looked for a solution to the PDE describing an asymptotic traveling wave: $Sg(x,t) = U(z)$, where $z = x + vt$ is a coordinate transformation into one dimension z. z reflects the new position of the wave after the passage of time t and rate of displacement v. The expression of the reaction-diffusion equation becomes:

$$\frac{v\partial U(z)}{\partial z} = D_{Sg}\frac{\partial^2 U(z)}{\partial z^2} + r\big(U(z)\big) \qquad (2)$$

This second order PDE can then be re-written as a system of first order differential equations. By letting $\frac{dU(z)}{dz} = M$, and substituting M back into equation 2, we get the following expression:

$$M = \frac{dU}{dz} \text{ and } vM = D_{Sg}\frac{dM}{dz} + r(U) \quad (3\ and\ 4)$$

Equation 4 can be approximated as a linear function of U by recalling that at the unreacted zone immediately preceding the wavefront, the far field condition $U(z) \xrightarrow[z \to -\infty]{} 0$ applies. We can therefore approximate the function $r(U)$ around $U = 0$ by performing a Taylor series expansion of $r(U)$ at this point and inserting the result into eqn. 4:

$$r(U) \approx r(0) + \frac{r'(0)U}{1!} = r'(0)U \quad (5)$$

Equation 4 becomes: $\frac{dM}{dz} = \frac{vM - r'(0)U}{D_{Sg}}$ and the final form of the system of 1st order differential equations becomes:

$$\frac{dM}{dz} = \frac{vM - r'(0)U}{D_{Sg}} \text{ and } M = \frac{dU}{dz} \quad (6\ and\ 7)$$

This system can also be rewritten back in terms of $U(z)$ as a homogenous constant coefficient 2nd order differential equation:

$$D_{Sg}\frac{d^2U}{dz^2} - v\frac{dU}{dz} + r'(0)U = 0 \quad (8)$$

The exponential solution to this ordinary differential equation will possess the roots of the characteristic equation as exponents. The characteristic equation is:

$$D_{Sg}g^2 - vg + r'(0) = 0 \quad (9)$$

$$g = \frac{v \pm \sqrt{v^2 - 4D_{Sg}r'(0)}}{2D_{Sg}} \quad (10)$$

The roots, g, must be real numbers so that the solution of $U(z)$ does not take negative values or exhibit oscillatory behavior. Therefore, the discriminant must be ≥ 0:

$$v^2 - 4D_{Sg}r'(0) \geq 0 \quad (11)$$

By rearranging equation 11, we obtain a requirement for the of the minimum velocity required to from a stable asymptotic traveling wave.

$$v \geq 2\sqrt{D_{Sg}r'(0)} \text{ and } v_{min} = 2\sqrt{D_{Sg}r'(0)} \quad (12 \; and \; 13)$$

It is important to note that the minimum rate of displacement does not depend on the initial conditions of the system. Additionally, $r'(0)$ can be determined for the for the autocatalytic circuit discussed previously in the absence of Sink:

$$r'(U(z)) = r'(Sg(x,t)) = \frac{\partial}{\partial Sg}[k_a C \times Sg] = k_a\left(C\frac{\partial Sg}{\partial Sg} + Sg\frac{\partial C}{\partial Sg}\right) \quad (14)$$

$$r'(0) = k_a C_{max}$$

$$v \geq 2\sqrt{D_{Sg}k_a C_{max}} \text{ and } v_{min} = 2\sqrt{D_{Sg}k_a C_{max}} \quad (15 \; and \; 16)$$

where the net reaction rate of Signal is differentiated with respect to Signal using the product rule and evaluated at [Signal] = 0; note that we assumed that at the leading edge of the wavefront where Signal approaches 0, Carrier takes its maximum concentration value, C_{max}. In the presence of Sink (Sk), $r'(0) = k_a C_{max} - k_a Sk_{max}$. This leads to the expressions:

$v \geq 2\sqrt{D_{Sg}(k_a C_{max} - k_d S k_{max})}$ and $v_{min} = 2\sqrt{D_{Sg}(k_a C_{max} - k_d S k_{max})}$ (17 *and* 18)

S6. Results & Discussion

Molar free energy change during strand displacement amplification:

The total Gibbs free energy change of the reaction can be expressed as the sum of the standard free energies of the species produced minus sum of the standard free energies of species consumed:

$$\Delta G_{rxn} = \sum_i y_i \, \Delta G^{\circ}_{product\ i} - \sum_i x_i \, \Delta G^{\circ}_{reactant\ i}$$

where ΔG_i° is the molar free energy of a particular DNA species and y_i and x_i are the number of moles produced or consumed during the reaction step. The total reaction for 1 cycle of amplification is:

$$Carrier + Fuel \xrightarrow{k} Signal + Output + Waste_3 \ (SI\ Rxn.S.1)$$

The molar Gibbs free energy for each species at 25 ºC in standard buffer conditions can be calculated using the nearest-neighbor model for DNA structural motifs[3], which assumes that the energy of the species is determined by the composition and locations of its base pairs. For DNA duplexes, each base-pair within the duplex is assigned a standard free energy based on the base pairing interaction (A-T/G-C), and the base-pairs directly adjacent to it to account for base stacking interactions. Additional factors for duplex stability accounted for by the model are the presence of terminal A-T and G-C pairings, the entropic penalty associated with nucleation of the first base-pair, and coordination of counter-ions with the backbone, which are all accounted for together with an initiation/terminal base-pairing term, and a symmetry term if the duplex is self-complementary. Together the standard free energy of each species can be expressed as:

$$\Delta G_i^{\circ} = \sum_j n_j \Delta G_j^{\circ} + \Delta G^{\circ}(init.term\ G-C) + \Delta G^{\circ}(init.term\ A-T) + \Delta G_{sym}^{\circ}$$

ΔG_j° is the standard free energy for the n_j possible base-pairs in the species. The values for these free energies have been computed and correlated across a variety of temperature and salt conditions[4–6]. Here, we used software tools, specifically NUPACK[7] to calculate the free energy of each species at standard reaction conditions; the NUPACK assumptions were 25 ºC in a buffer containing 12.5 mM Mg^{2+} and 1 M Na^+.

$$\Delta G^\circ_{Carrier} = -72.43\ kcal\ mol^{-1}$$

$$\Delta G^\circ_{Waste_3} = -73.10\ kcal\ mol^{-1}$$

$$\Delta G^\circ_{Signal} = -2.21\ kcal\ mol^{-1}$$

$$\Delta G^\circ_{Output} = 0.0\ kcal\ mol^{-1}$$

$$\Delta G^\circ_{Fuel} = -2.21\ kcal\ mol^{-1}$$

y_i and x_i = 1 for all species in SI reaction S1. Therefore, we expect $\Delta G_{rxn} = -0.67\ kcal\ mol^{-1}$ for the completion of 1 cycle of amplification at 25º C in the presence of 12.5 mM Mg^{2+}. For comparison, the average molar thermal energy fluctuation from molecular collisions at 25 ºC is $kT * N_A = 0.59\ kcal\ mol^{-1}$, where k is the Boltzmann constant and N_A is Avogadro's number, illustrating how close the free energy change of the system is to the energy provided by random molecular collisions.

Measurement of Amplifier Rate Constants

We first fit reaction rate constants in well-mixed conditions for the un-thresholded amplifier. The fitted parameters were the reaction rate constants k_a, k_r, k_{rep} and k_i shown in the main text reaction diagram Figure 6. The strand displacement mechanism for the reaction of Fuel and Intermediate and Signal and Intermediate occur through the same toehold and involve branch migration along specificity domains of roughly equal length, so we assumed that the rate constants k_r and k_i were equal in our model. The average values for the fitted parameters are

listed in **Table S2** and the least-squares fit for each reaction is plotted as a dashed line in main text Figure 8. We observed that the estimated magnitudes of k_{rep}, k_r and k_i from the model were within an order of magnitude of known experimental ranges for reactions with the corresponding toehold sizes. The expected magnitudes of 7 nucleotide, 6 nucleotide, and 4 nucleotide toehold bimolecular rate constants are 3E6 M^{-1} s^{-1}, 5E5 M^{-1} s^{-1}, 5E3 M^{-1} s^{-1} respectively[8]. Interestingly, the magnitude of fitted rate constant k_a (which involved a 5 base-pair toehold ~ 10^4 M^{-1} s^{-1}) was higher than the expected value by a factor of 10. Additionally, the measured leak rate constant for the leak reaction between Fuel and Carrier was ~ 10^3 M^{-1} s^{-1}, roughly 2 orders of magnitude higher than the value previously reported by Zhang et al.[9]. As a result of the overestimated reaction rate constants, predicted kinetic traces fail to recapitulate some of the sigmoidal character observed in the experimental curves. Key differences exist between the purity of the strands used in their experiments and in our experiments. Zhang et al. used HPLC purified DNA. All non-modified strands purchased from IDT in our experiments were ordered with standard desalting, which can yield a higher fraction of oligonucleotides with 5'end nucleotide deletion errors than what is found in HPLC purified DNA. 5' deletion errors could expose bases at the end of the 4b' domain of Carrier, effectively creating a permanent 1 or 2 nucleotide toehold for Fuel to hybridize to, in addition to the Carrier nick, and opposite duplex end which both offer possible invasion points for Fuel. These toeholds could account for the higher observed reaction rates. Finally, subtle differences also existed between the duplex purification protocols used in both experiments. Zhang et al. purified DNA duplexes using 12% non-denaturing polyacrylamide gel electrophoresis gels using a power of 180V for 6 hours. Our protocol used 15% non-denaturing polyacrylamide gel electrophoresis gels run at 150V for 3 hours.

Similarly, the average rate constants fitted to the thresholded amplifier data yielded a similar trend to what was observed with the unthresholded system. Here, we fit k_a, k_r, k_{rep}, k_i, k_{leak}, and k_t. We observed that the magnitudes of k_r and k_i were in the expected range for a 4-nt toehold reaction. However, the predicted magnitude of k_a was an order of magnitude higher than its expected value. Additionally, k_{rep} was one order of magnitude lower than the expected rate constant for a reaction involving a 7 nucleotide toehold rate constant ~ 10^6 M^{-1} s^{-1} while k_t was on the expected order of a 7 nucleotide rate constant. Finally, the magnitude of k_{leak}, which was 85 M^{-1} s^{-1}, fell within the expected range for a reaction involving a 0-2 nucleotide toehold ~ 10-100 M^{-1} s^{-1}. It is important to note that during purification of the Carrier complex, it was incredibly difficult to ensure consistency in the fraction of properly formed complex; different experiments used different batches of purified Carrier. Variation between these results across data sets may be attributed to differences in Carrier purity from batch to batch as was observed by Zhang et al.[9].

The well-mixed models do not consider partially exposed domains or shortened toeholds caused by truncation errors in DNA synthesis which could result in exposed nucleotides on a DNA duplex and slower rates of reaction. We also considered two additional leak pathways that involved toehold occlusion: the reaction of Signal with Waste 3 and the reaction of Signal with Reporter to form additional waste complexes. Each reaction involved the hybridization of part of Signal to a 7-nucleotide (nt) toehold. The Signal/Waste 3 reaction involved branch migration to form a 3-stranded intermediate species. Since toehold occlusion and branch migration states could result in the Signal being trapped in a 3 strand complex and thus slow amplification by acting as a sink for Signal, we examined whether these side reactions influenced the overall

amplification dynamics. The effective unimolecular rate constants for these class of reactions has been established in the literature. The rate constant of Signal dissociation from a 7-nt toehold is:

$$k_{off1} = k_{on1} e^{\frac{\Delta G^{\circ}}{RT}} = 0.54\ s^{-1}$$

where ΔG° is the free energy of a 7-nt toehold (-9.2 kcal mol^{-1}) and k_{on} = 3E6 $M^{-1}s^{-1}$. The rate of Signal

dissociation from Waste 4 is:

$$k_{off2} = k_{on2} \frac{1}{X} e^{\frac{\Delta G^{\circ}}{RT}} = 0.027 s^{-1}$$

where k_{on} = 5E4 M^{-1} s^{-1}, ΔG° = -6.9 kcal mol^{-1}, and X is a correction term for the number of branch migration states in the 3-strand complex. For Waste 4 for which is formed from the hybridization of Signal and Waste 3, X is 16 and k_{off2} = 0.027 s^{-1}. We incorporated these rate constants and leak reactions into our model and observed no improvement in the predictions with the added leak reactions compared to those without them (Figure S2). We also tried fitting the unimolecular rate constants for two reactions and again observed no improvement in predictions. Fitted values of k_{off1} and k_{off2} were 0.30 s^{-1} and 0.35 s^{-1}. It is possible that a subset of improperly annealed complexes in addition to truncation errors yield some fraction of the reactant species that are defective or react more slowly, which could explain experimental deviations at lower Carrier concentrations. Experimentally, care was taken during plating of the strand displacement reaction to aliquot the reactants as quickly as possible in order to measure the complete evolution of the system as it emerged from its lag phase. Errors due to residual liquid retention in pipette tips, and time spent loading the qPCR plate after triggering the reaction are also potential sources of deviation.

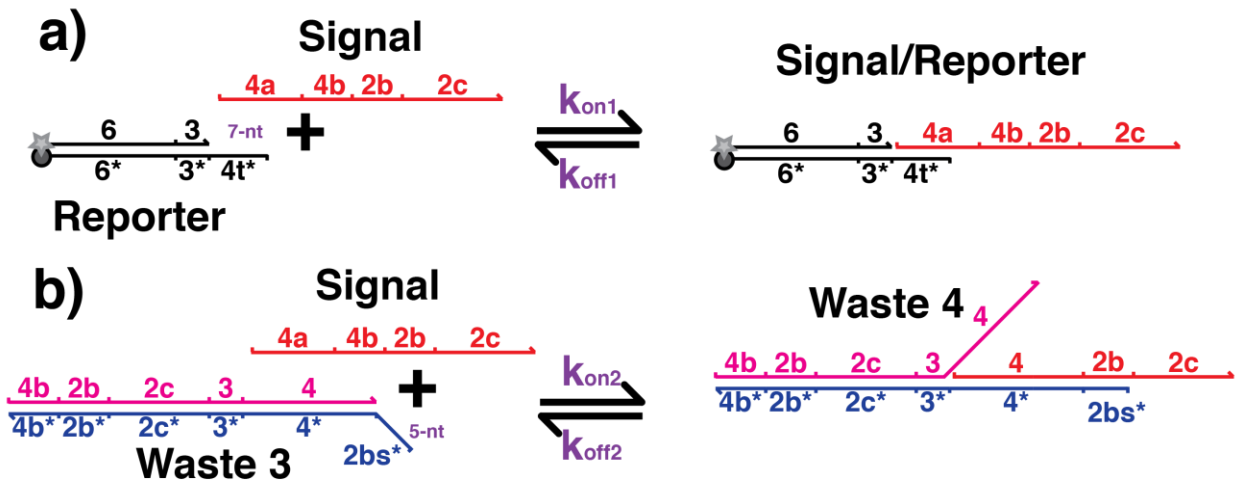

Figure S2: Additional amplifier leak reactions considered in well-mixed models. Neither reaction was observed affect regression.

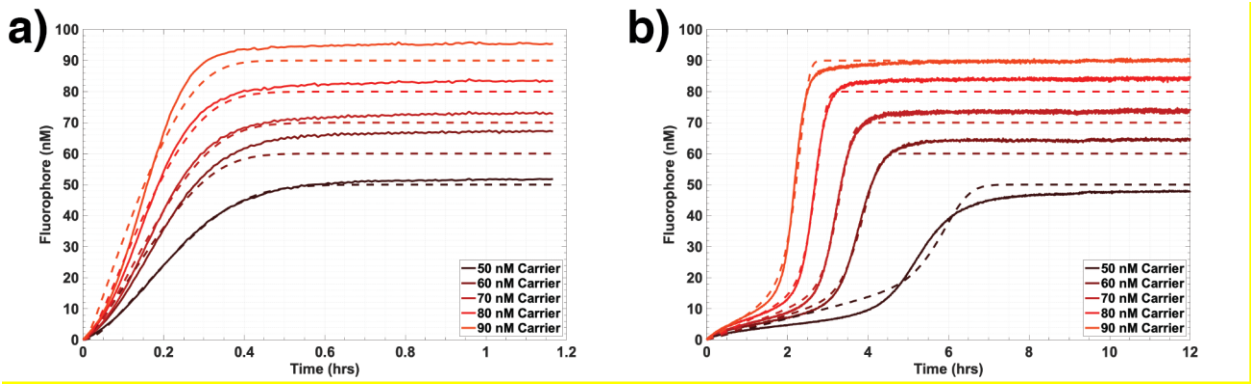

Figure S3: Refitting of main text Figure 8 while incorporating the leak reactions illustrated Figure S2.

Table S2: Un-thresholded and thresholded amplifier average fitted rate constants (95% confidence intervals)

	ka	kr	ki	kt	krep	kleak
0 nM Sink	1.9E5 ± 1.5E4 M^{-1} s^{-1}	8.9E3 ± 1.6E2 M^{-1} s^{-1}	8.9E3 ± 1.6E2 M^{-1} s^{-1}	N/A	1.8E5 ± 1.5E5 M^{-1} s^{-1}	2.9E3 ± 5.0E2 M^{-1} s^{-1}
50 nM Sink	1.2E5 ± 3.2E4 M^{-1} s^{-1}	6.8E3 ± 1.8E3 M^{-1} s^{-1}	6.8E3 ± 1.8E3 M^{-1} s^{-1}	3.8E6 ± 2.4E5 M^{-1} s^{-1}	9.7E5 ± 1.1E5 M^{-1} s^{-1}	8.5E1 ± 1.4E0 M^{-1} s^{-1}

Table S3: Average fitted rate constants for thresholded amplifier perturbation experiments (95% confidence intervals).

	ka	kr	ki	kt	krep	kleak

20 nM Signal Addition	2.6E6 ± 1.5E6 M^{-1} s^{-1}	4.7E3 ± 2.5E3 M^{-1} s^{-1}	4.7E3 ± 2.5E3 M^{-1} s^{-1}	5.8E5 ± 6.4E5 M^{-1} s^{-1}	3.9E4 ±2.0E4 M^{-1} s^{-1}	1.1E2 ± 4.8E1 M^{-1} s^{-1}
20 nM Sink Addition	1.6E6 ± 5.4E5 M^{-1} s^{-1}	1.2E4 ± 2.6E4 M^{-1} s^{-1}	1.2E4 ± 2.6E4 M^{-1} s^{-1}	9.4E5 ± 6.3E5 M^{-1} s^{-1}	2.0E6 ± 2.3E6 M^{-1} s^{-1}	1.3E1 ± 1.1E1 M^{-1} s^{-1}

Fitted rate constants for the perturbation experiments are listed in **Table S3**. We observed that the optimized magnitudes for the rate constants corresponded to toehold sizes that were within 2 nucleotides of with the actual sizes involved in the experimental system.

Idealized autocatalysis with 5 nucleotide toeholds

In main text Figure 11, we observed that the stand displacement reaction implemented with a 5 nucleotide (nt) autocatalytic rate constant fails to produce a pulse. In the idealized waveguide models, when we reduced the rate constant for the single step autocatalytic reaction from 2E5 M^{-1} s^{-1} to 5E4 M^{-1} s^{-1}, which corresponds to a reduction in toehold length from 6 nt to 5 nt, the waveguide failed to produce a pulse over the range of concentrations originally used in those models. However, by further increasing the reactant concentrations, the waveguides were able to propagate pulses super-diffusively. Specifically, we increased the starting Signal and Carrier concentrations to 220 nM and 780 nM respectively. The Sink concentration within the insulation was increased to 1500 nM. In the absence and presence of 70 nM Sink sequestered in the waveguide core, $\alpha = 2.04 \pm 0.01$ and 2.06 ± 0.02 respectively (95% confidence interval), which indicated that the waves achieved superdiffusive behavior (Figure S4). Adjustment of the reactant concentrations informed our strategy for inhomogeneous patterning to suppress the leak reaction in the strand displacement simulation.

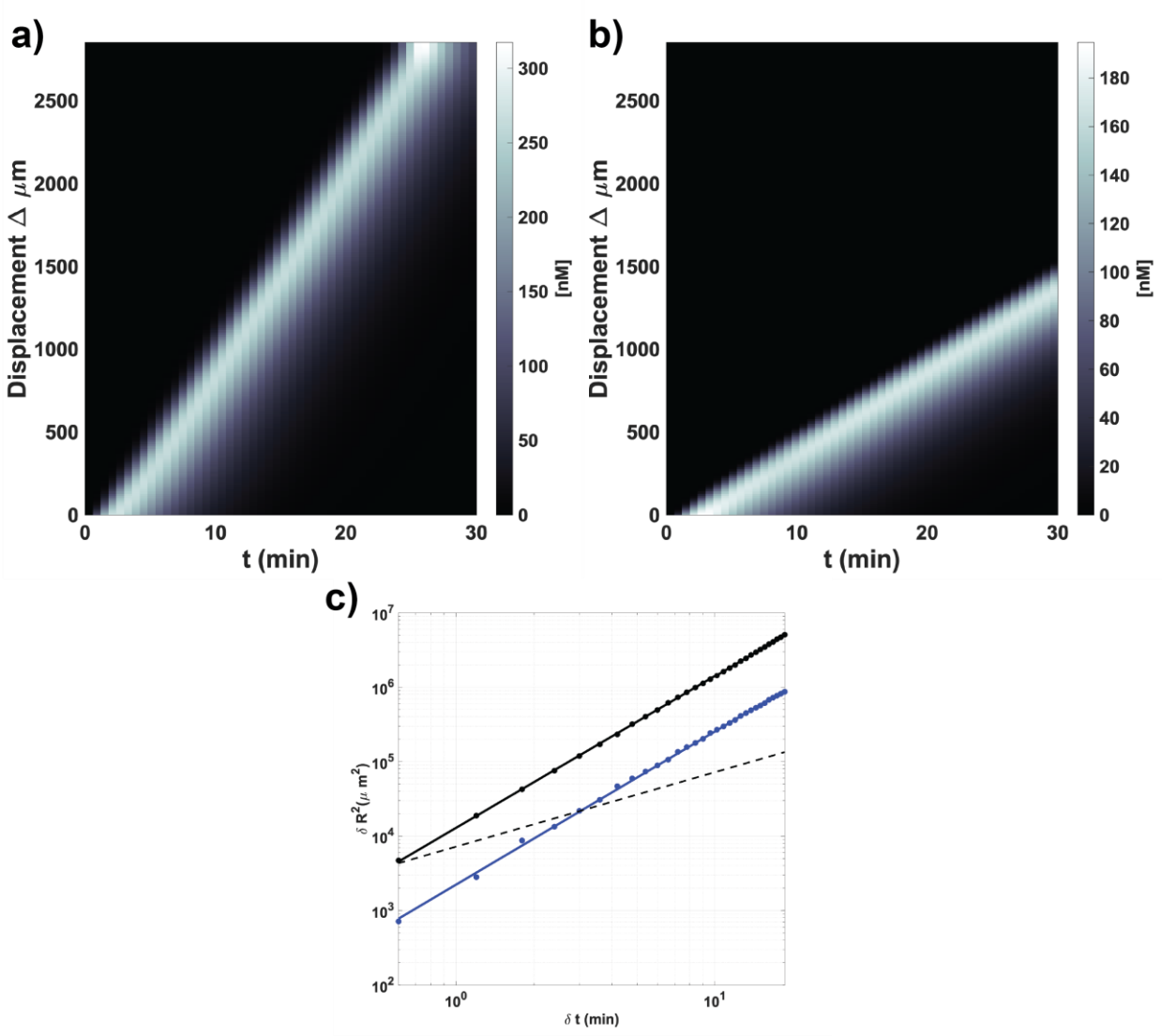

Figure S4: Kymographs of idealized amplification in (a) 0 nM Sink and (b) with 70 nM Sink within the waveguide path. c) Square of wavefront displacement vs. time for 0 nM Sink (black) in the waveguide path, 70 nM Sink within the waveguide path (blue), and diffusion of a 42-nt sized oligonucleotide (black dashed line). The range of time points analyzed in c) was 5.4 minutes to 24 minutes.

Assessment of a Photoprotection Strategy for prevention of Carrier-Fuel leak reactions

As a first attempt to mitigate the leak reaction between Carrier and Fuel in the amplification reaction, we chose to add 7-bp clamp domains to both ends of the duplex that had no complementarity to Fuel. To prevent Fuel from reacting with Carrier, we extended the length of Signal and Output to contain the reverse complement of the 7 nucleotide domains added to the bottom strand of Carrier (referred to as Carrier_B). Importantly, the original unclamped sequence

structure of Signal and Output, and $Carrier_B$ was retained. The toehold of $Carrier_B$ and 4a domain of Signal formed bulge loops (**Figure S7**) in the duplex. The hypothesis of this design was that: 1) the presence of clamps would slow the rate at which Fuel could nucleate with frayed bases at the ends of $Carrier_B$ due to steric hindrance, and that 2) during partial displacement of Signal or Output by Fuel, the clamps would increase the rate of rehybridization and reverse branch migration of Signal and Output because these molecules possess a domain to reattach and/or remain attached to Carrier duplex, thereby forcing these oligos into a set of conformational configurations that lower the energy barrier for base nucleation with adjacent segments of Fuel-hybridized duplex. During the photo-deprotection process, Signal and Output would be attached to their clamp domains with 1-(2-nitrophenyl) ethyl linkers (**Figure S7**). Exposure of Carrier to UV light would break these linkages and produce the functional form of Carrier where Signal and Output can be fully displaced from the complex during strand displacement. To verify that the protected form of Carrier, $Carrier_p$, reacted with Fuel at a slower rate or did not react at all, we first mixed 50 to 90 nM $Carrier_p$ with 200 nM Fuel and 150 nM Reporter in different reaction wells of a 96 well plate. We tracked the increase in Fluorophore concentration over time (**Figure S8**) and observed a slow and gradual increase in Fluorophore concentration, where the rate of increase over time appeared to be proportional to the initial Carrier concentration. Additionally, all kinetic traces maintained their concavity and no inflection points were visually observed over the timescale of measurement, suggesting that autocatalysis was inhibited and the rate of Fluorophore production was largely coupled to the bimolecular reaction of Fuel and $Carrier_p$. Based on these observations, we designed an ODE model of the reaction which assumed that autocatalysis was inhibited (i.e. Signal could not react with $Carrier_p$) and that Fuel was able to react with $Carrier_p$ to produce Output (see Supporting Information: Materials & Methods for

model equations). Nonlinear least-squares regression was performed to fit the model to the experimental data: k_{leak} and k_{rep} were the fitted parameters. The average values of k_{leak} and k_{rep} were 22 ± 1.9 M^{-1} s^{-1} and 2.8E6 ± 1.5E6 M^{-1} s^{-1}, which were within one order of magnitude of values obtained from previous fitting analyses of the leak and reporting reaction rates.

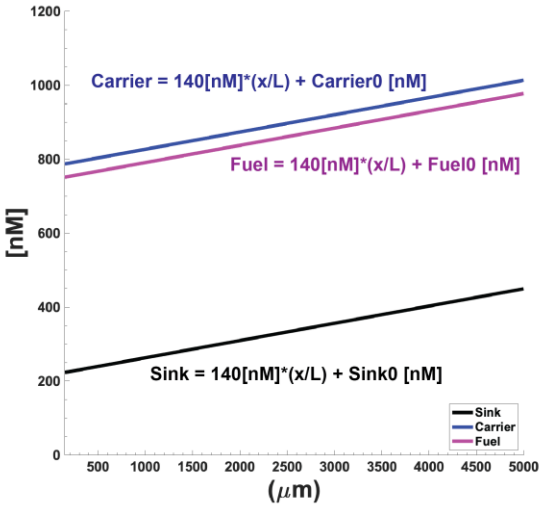

Figure S5. Initial concentration gradients of Carrier, Fuel, and Sink employed in the gradient patterned DNA reaction-diffusion waveguide.

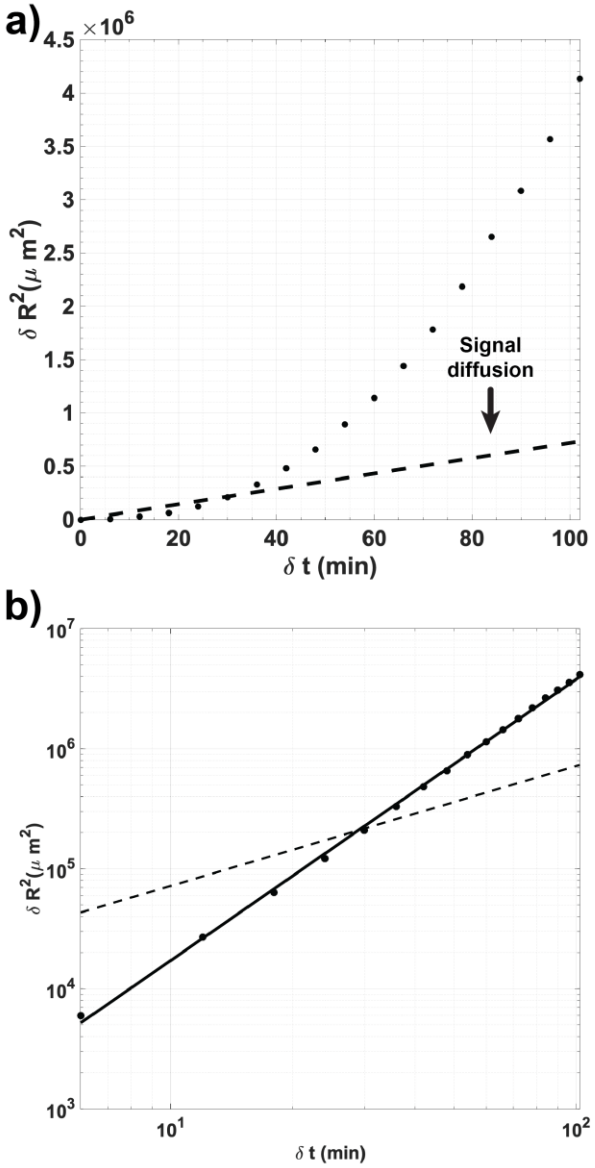

Figure S6. Relative wave displacement vs. time. a) Linear scale. b) Log-log scale. Black circles are results of PDE reaction-diffusion model and the solid black line represents the line-of-best-fit. Average slope = 2.34 ± 0.04 (95% CI). Black dashed lines in a) and b) indicate the expected mean-squared displacement for diffusion of a 42 nucleotide DNA molecule. The simulated time window analyzed here is 8.2 hrs - 9.9 hrs in the Comsol model.

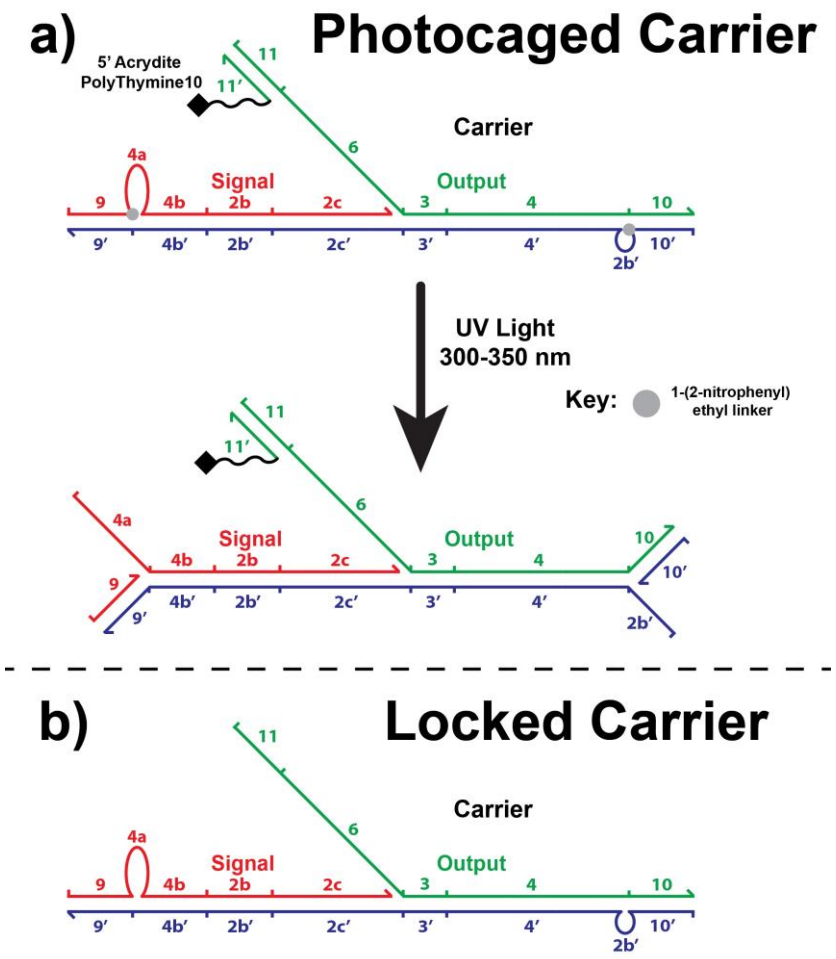

Figure S7. a) Carrier photoprotection strategy using nitrobenzyl-modified clamp domains to prevent Fuel leakage with Carrier duplex ends. Photocleavage of 1-(2-nitrophenyl) ethyl linkers results in exposure of the 2b' toehold on Carrier and the activation of bound Signal. b) Locked Carrier substrate tested in well-mixed experiments for its ability to slow the Fuel-Carrier leak reaction.

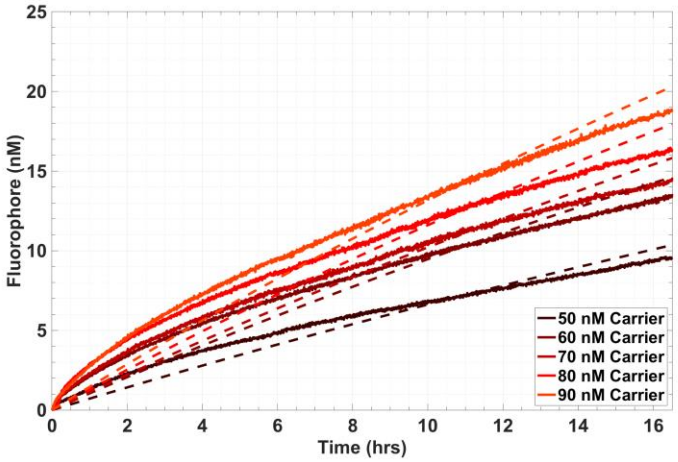

Figure S8. Fluorescence signals generated from incubation of 50-90 nM Locked Carrier with 200 nM Fuel.

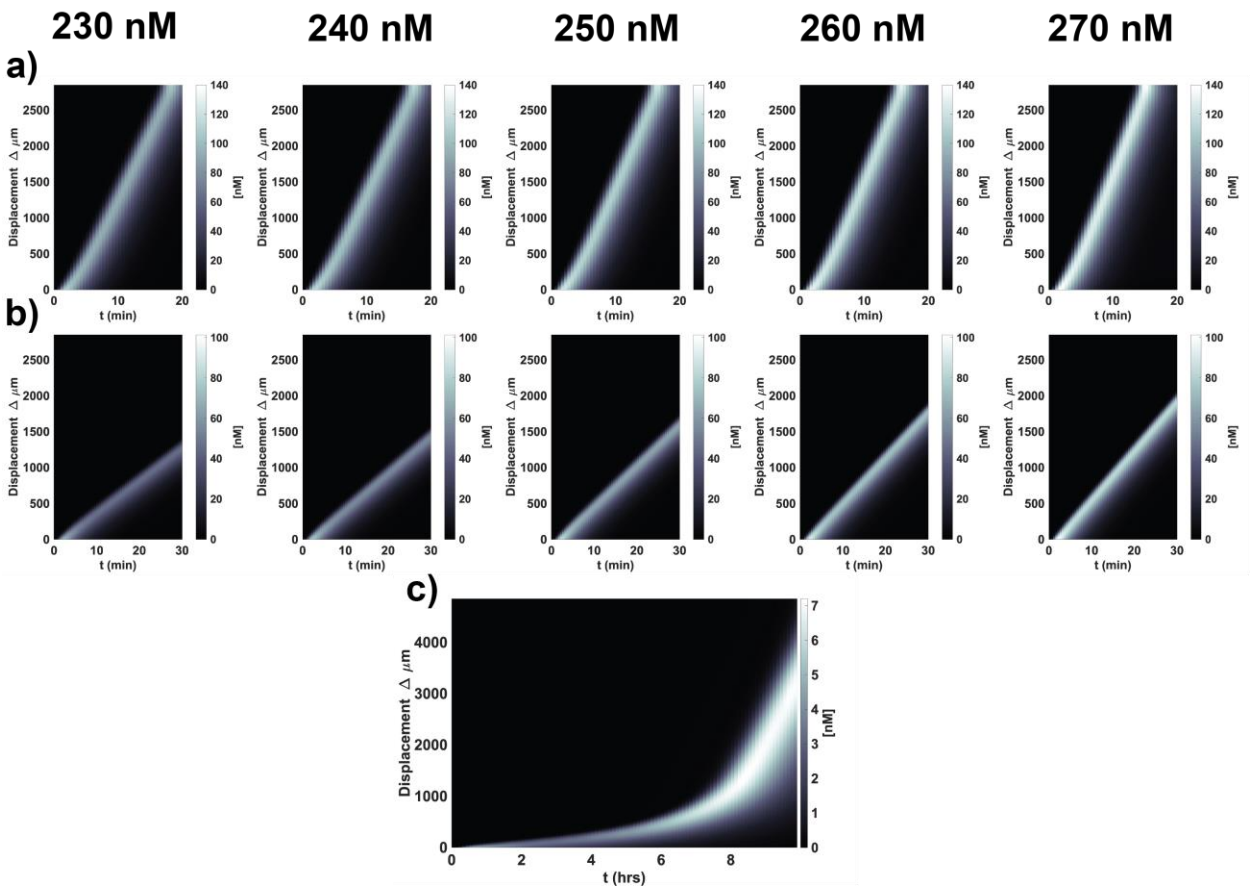

Figure S9: Kymographs of wave displacement as a function of Carrier concentration in a) an idealized waveguide (6 nt toehold) without any Sink, b) an idealized waveguide (6 nt toehold) with 35 nM Sink present, and c) within the autocatalytic DNA strand displacement waveguide with gradient patterning of Sink, Carrier and Fuel to mitigate the leak reaction.

Wave displacement and size using inhomogeneous patterning of reactants

For the DNA strand displacement simulation using inhomogeneous reactant concentrations, the width of the pulse gradually increases as it traverses the waveguide (Figure S5, Figure S6, and Figure S9). The net rate of Signal accumulation is much lower in the strand displacement model compared to the idealized systems. Unlike the idealized model which did not incorporate the Carrier Fuel leak reaction, Signal production and degradation occur along the waveguide's path. Carrier, Fuel, and Sink concentrations decrease over time prior to the arrival of the wave. As Sink is consumed in order to suppress the leak reaction, it becomes easier for the pulse to propagate through that particular section compared to a system where the concentration

of Sink is static; less Sink is present to impede wave displacement over time. Unlike the idealized simulations (Figure S9a-b, Figure S10), the pulse does not encounter the same concentration of Sink at its leading-edge during propagation, which allows it to widen as it travels. Additionally, the pulse dynamics are a function of local reactant concentrations due to the time dependence of Carrier, Fuel, and Sink in untriggered parts of the waveguide which affects the rate of displacement over time as shown in Figure S9c.

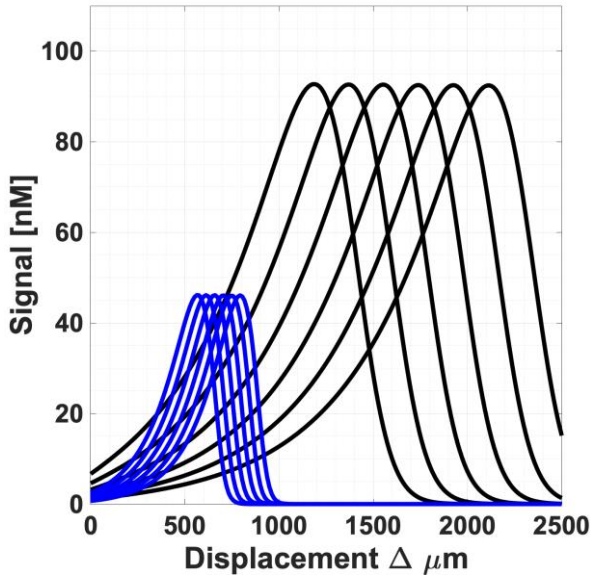

Figure S10: Signal concentration profiles for an idealized autocatalytic waveguide (6 nt toehold) with 0 nM Sink (black) and 35 nM Sink (blue) patterned along the waveguide path.

References

(1) Dorsey, P. J.; Rubanov, M.; Wang, W.; Schulman, R. Digital Maskless Photolithographic Patterning of DNA-Functionalized Poly(Ethylene Glycol) Diacrylate Hydrogels with Visible Light Enabling Photodirected Release of Oligonucleotides. *ACS Macro Lett.* **2019**, *8* (9), 1133–1140.

(2) Shampine, L. F.; Reichelt, M. W. The MATLAB ODE Suite. *SIAM J. Sci. Comput.* **1997**, *18* (1), 1–22.

(3) SantaLucia, J. A Unified View of Polymer, Dumbbell, and Oligonucleotide DNA Nearest-

Neighbor Thermodynamics. *Proc. Natl. Acad. Sci.* **1998**, *95* (4), 1460 LP – 1465.

(4) Frank-Kamenetskii, M. D. Simplification of the Empirical Relationship between Melting Temperature of DNA, Its GC Content and Concentration of Sodium Ions in Solution. *Biopolymers* **1971**, *10* (12), 2623–2624.

(5) Erie, D.; Sinha, N.; Olson, W.; Jones, R.; Breslauer, K. A Dumbbell-Shaped, Double-Hairpin Structure of DNA: A Thermodynamic Investigation. *Biochemistry* **1987**, *26* (22), 7150–7159.

(6) Rentzeperis, D.; Ho, J.; Marky, L. A. Contribution of Loops and Nicks to the Formation of DNA Dumbbells: Melting Behavior and Ligand Binding. *Biochemistry* **1993**, *32* (10), 2564–2572.

(7) Zadeh, J. N.; Steenberg, C. D.; Bois, J. S.; Wolfe, B. R.; Pierce, M. B.; Khan, A. R.; Dirks, R. M.; Pierce, N. A. NUPACK: Analysis and Design of Nucleic Acid Systems. *J Comput Chem.* **2011**, *32* (1), 170–173.

(8) Zhang, D. Y.; Winfree, E. Control of DNA Strand Displacement Kinetics Using Toehold Exchange. *J. Am. Chem. Soc.* **2009**, *131*, 17303–17314.

(9) Zhang, D. Y.; Turberfield, A. J.; Yurke, B.; Winfree, E. Engineering Entropy-Driven Reactions and Networks Catalyzed by DNA. *Science (80-.).* **2007**, *318* (5853), 1121–1125.